Structural Design of a 64-Meter Low-Cost Antenna

M. S. Katow
DSN Engineering Section

The computer model of a 64-m ground antenna was almost completely generated by 1108 software. The reflector and alidade model was iteratively designed and analyzed by the JPL/IDEAS program, which minimized the distortion RMS with respect to the structural weight. Curves of values describing the optimizing processes are presented, functional aspects of the structural elements are defined, and detail descriptions of the design equations for stress calculations are included. Computed data used for calculating the RF boresight error and natural frequency answers are also included.

I. Introduction

The computer analyses of the 60-, 80-, and 100-meter reflector structural assemblies and their corresponding alidades were supplied to our cost analyzing contractor. The computer analyses were output from the JPL/IDEAS and NASTRAN programs.

This study was a follow-on of work done in Refs. 1 and 2 with the goals of supplying usable details for calculating performances and the manufacturing and erection costs of the antennas. This article describes what design considerations were used to generate the 64-m models and control the designing cycles through the IDEAS program to result in performances that satisfy the specifications.

At the time of this study, the design objective was to maintain or surpass the 64-m MARS' performance with lower costs.

With the emphasis on building more cost effective Deep Space Station antennas, we concluded that the design concepts pioneered by the Bonn antenna designers, using the axial symmetric reflector structure and the efficient four wheel alidade, most satisfactorily fulfills the performance requirements of the antenna at the lowest fabricated cost as discussed in Ref. 1. The elimination of the master equatorial pointing system makes the symmetrical design possible.

The JPL/IDEAS (Ref. 3) program was used to iteratively design the reflector and alidade truss structures. The design objective of the reflector structure was to minimize, by changes in the cross-sectional areas of the truss bar members the RMS distortions of the surface panels connecting nodes for wind and gravity loadings. For the alidade, the objective was to minimize RF boresight changes from the wind loading.

To emphasize the importance of accurate surface panels for X-band antennas, the accuracies and manufacturing steps are described for the surface panels installed on the 64-m DSS-14 antenna.

The NASTRAN (Ref. 4) structural program was used in the alidade analyses where rotations of structural members were

desired at the node points. That is, beam elements with bending formulation were needed instead of pin jointed bars used in IDEAS analyses. However, the design for optimum cross-sectional areas of the alidade members was done by using the "point" mode in the IDEAS program. Here, the compliances of the two mounting points of the reflector were minimized with constraint on the total structural weight of the alidade, with the objective of minimizing the RF boresight shift.

As done before (Ref. 1 and 2), a data generating program was used to prepare the reflector model. The cassegrain primary feed cone, the center hub portion of the reflector, the reflector back-up cone, the "stick" quadripod, the elevation wheel structure and the alidade were hand generated.

II. Reflector Configuration

The primary function of the reflector's truss assembly is to provide stable support points for the paraboloidal reflective surface panels under the environmental loads. Ideally, the best or most uniform deflection is obtained when the support points of each surface panel are on main rib trusses only. However, this truss arrangement would be the most expensive. The trade-off for lower costs is to create support points in the hoop truss and use intermediate ribs to provide the midpoint support points (Fig. 2). Of course, the additional deflections of these nonmain rib supports must be a reasonable fraction of the total desired distortion RMS.

The surface area or size of a surface panel maximized for the desired deflection under the environmental loads results in the minimum number of main ribs. The panels fabricated for the 64-m antenna at DSS 14 used aircraft-type beams for the framework, which resulted in lightweight and stiff panels. Although the surface sheets were riveted to the beam framework, spot welded fastenings or epoxy cemented joints are preferred to eliminate joints in the reflective surfaces that may result in RF noise bursts.

As the size of the surface panels increase, the distortions from the manufacturing processes, and the gravity and air pressure loads will also increase. Some points on the curve "of size vs accuracy" from manufacturing are illustrated by the surface panels built for the 64-m DSS 14 antenna (Table 1 and Fig. 1).

A static load test was made using bricks for weights. Specifically, panel No. 4 (Table 1) was supported top down from an angle iron framework using the normal supporting screws. Bricks equivalent to 1340 N/m^2 (28 lb/ft^2), the expected upward pressure at a 53.6-m/s (120-mph) wind speed, were placed on the panel. The maximum recorded deflection was 4.37 mm (0.172 in.) with the bottom cross straps on, and 5.08 mm (0.200 in.) with the straps off. For the 13.4-m/s (30-mph) air speed load, the maximum deflection was 0.48 mm (0.019 in.). The 50% porosity of the reflective surface was accounted for in the pressure difference calculations. Also, the zero returns of the dial indicators showed that the panels were not stressed to yield for the stow air loads.

The manufacturing process used a fixture with an egg-crate type of frame contoured on top to fit the panel's surface curvature, and a flat sheet of 2.36-mm (0.093-in.) thick aluminum was placed on the frame. Next, the Z-shaped aluminum beams, contoured to the correct curvature by rolling, were placed on top to force the flat sheet to the curvature of the fixture as the beams were pressed against the fixture. With clamps holding down the beams, pilot holes for the rivets were drilled and filled with temporary rivets. The panels were then moved to the automatic riveting machines for applying the rest of the rivets.

Each manufactured panel was placed in a contour checking fixture and held in place at the six fastening points to the reflector structure. The contour error for every 645 cm^2 was read and recorded on IBM punched cards. These cards were input to a computer; the root-mean-square (RMS) evaluations are shown in Table 1. The overall manufacture RMS error for all of the panels was 0.89 mm (0.035 in.).

Inspection of the error pattern of all panels showed that the error was not randomly distributed. It was a result from stressing of the beams by the surface sheet as it tried to return to its originally flat surface. In other words, the curvature readings showed a general flattening of all panels or a definite high point near the center. The vendor has improved his manufacturing techniques where more accurate panels were required by either over rolling the beams to a smaller radius curvature, or stretch-press forming the surface sheets to the correct curvature before the assembly process.

From the foregoing, it was concluded that surface panels up to 8.00 m^2 could be manufactured to 0.5 mm RMS accurately. Also, their stiffness from air loading tests showed that negligible distortion RMS needed to be added for air speeds up to 13.4 m/s (30 mph).

The radial rib type of reflector structure easily satisfied the axial symmetric configuration required for minimum gravity loading distortions. As shown in Fig. 3, with the two supporting points ② and ③ on the symmetric axis, all points on a particular hoop should deflect the same amount for gravity loading in the direction of the axis, if axial symmetry is satisfied. By proportioning the cross sectional areas of the main rib truss and accounting for the hoop-member areas, the

top nodes could be made to deflect to another parabola of longer focal length for the symmetric gravity loading case. Thus, the distortion from the symmetric loading case can be made negligible.

The antisymmetric loading produces opposite direction distortions in the top and bottom halves of reflector if gravity loading at horizontal look is considered. Here, the depth of the ribs has a major effect on the magnitude of the displacements, but some minimization is done in the IDEAS program arranging or changing the radial distribution pattern of the cross-sectional areas at the same time the minimization is done for the symmetric load case.

The number of main ribs of the low-cost 64-m antenna was decreased by a factor of two over the 64-m antenna at DSS 14, and the mounting points for the surface panels were created by adding subtrusses as shown in Fig. 2, Section GG, and in Fig. 3, Sections AA and BB.

The reflector structure (Fig. 3) was completed by adding a back-up cone consisting of bars from the connection node (3) to alternate main ribs at the bottom of the fifth hoop, and a bar from nodes (2) to (3). Node (3) thus becomes a very "hard" node and capable of becoming a support point for both axial and lateral directions. The balancing counterweight of the reflector about the elevation axis is located here at node (3).

The computer model of the reflector's truss structure is a half (1st and 4th quadrants) model with normally symmetric constraints on the symmetry plane. For the supporting nodes, node (2) is constrained laterally (X and Y of Fig. 3) only. Node (3) is constrained both laterally and axially (Z of Fig. 3).

III. Elevation Wheel/Alidade Configuration

The two base or mounting nodes of the reflector are fastened to nodes (2) and (3) of the elevation wheel/alidade assembly shown in Fig. 4. Nodes (2) and (3) are in the center part of the inverted-pyramid-shaped truss of the elevation wheel assembly with the elevation bearing shafts at nodes (5) and (6). The elevation gears (shown as dotted lines) are fastened to a truss assembly attached to nodes (3), (7), and (8). Nodes (5) and (6) with (7) and (8) can support a quadripod separated from the reflector structure (shown with dashed line to node (9)).

The base of the alidade is a square frame with two cross diagonals and the azimuth radial bearing is located at the intersection of the diagonals. Attached to each corner are a set of wheels that rides a circular rail. To the two sides of the square base, triangular trusses are attached ((5), (50), (52) and (6), (54), and (55)) that support the elevation bearings located at (5) and (6). The lateral supports for the two triangular trusses are from bars (5) – (51) and (6) – (51). With only lateral constraints supplied by a cylindrical-type roller bearing in the azimuth radial bearing at (51) and axial fixity at the elevation bearings as supplied by spherical roller bearings, the elevation wheel/alidade assembly becomes a stable determinant truss with special characteristics.

The torsional rigidity of the alidade assembly itself about the X and Y axes are low even with the pentahedron shaped truss (50), (52), (54), (55), and (53) in place. The basic rigidity of the alidade about these axes results from the azimuth bearing wheels at the four corners in contact with the azimuth rail with preloads available from the dead weights. The components of forces on nodes (2) and (3) in the Y direction are transferred through the elevation bearings, the side triangular trusses of the alidade and then to the radial bearing, with components to the wheels at the base corners. Forces in the X direction are also directed through the elevation bearings, but now into the inclined bars (5) – (51) and (6) – (51) and to the azimuth radial bearing with components into the side triangular trusses and the azimuth wheels. Since the radial bearing at (51) cannot resist vertical axial loads, the axial forces in the inclined bars must be equal, but opposite in sign and, hence, the axial thrust or X loads in the two elevation bearings will be equal. Also, thermal expansion of the elevation wheel truss with respect to the alidade truss does not induce thermal stresses. Compensation is made when the azimuth radial bearing moves axially.

The remaining portion of forces in the Y direction is passed through link (3) – (53), representing the elevation gear-boxes, into the pentahedron shaped truss, and then to the base frame of the alidade.

By separating the antenna into two truss assemblies connected at only two nodes, the reaction forces from the reflector assembly analysis can be used as loads for the elevation wheel/alidade assembly analysis. However, it is also possible to attach the elevation wheel assembly to the reflector and analyze the reflector with constraints at nodes (5) and (6) with fixed cross-sectional areas for the wheel members.

By the first method, the reflector members can be designed for minimum RMS distortion of the reflector geometry while maintaining structural strengths for the maximum wind loads in the IDEAS program. Then the elevation wheel/alidade assembly can be designed for minimum compliance of the reflector's mounting nodes (2) and (3) using the "point"

mode in IDEAS. However, the forces transmitted between the reflector and elevation wheel must be separated as analyzed. In other words, all axial or Z forces should be transferred at node ③ while maintaining axial rigidity of only the bar ② – ③ used for the reflector analysis.

Another solution is to attach the elevation wheel to the reflector and check analyze the axial rigidity requirements of bar ② – ③. Bending compliances of the elevation wheel beams must be accounted for in the final solution.

IV. Structural Details Discussion

The 64-m reflector truss assembly was configured for eight rows of surface panels, with the fifth hoop at the 50% diameter. The outer panel has a hoop at its midpoint to maintain an efficient triangular truss configuration (Fig. 3). Several preliminary IDEAS analyses indicated that any increase of the center depth of 3.81 m (150 in.) and the edge height of 1.52 m (60 in.) showed minimal decrease in wind distortion for the extra size.

To minimize wind torques about rotation axes, the vertical distance between the vertex of the paraboloid and the elevation bearing axis should also be minimized. A 2.08-m centerline distance below the reflector was defined to allow sufficient space for maintenance work on the elevation bearing assembly.

The bottom chord of the main girder was configured to be flat and horizontal. This places node ② above the elevation axis centerline. If a box beam is utilized in the elevation wheel, its depth would necessarily place the connection node ② above the centerline of the elevation bearing axis, even for a straight box beam. If necessary, the bottom chords of the main ribs could be dropped in the center for better match up of the pieces. In any case, a bending moment as well as the bending stiffness must be accounted for in the top members of the elevation wheel truss as to their effects on the gravity load distortion of the reflector. This check between the computer models and the actual field members needs to be carefully studied for members joining node ②.

Another node having physical interference problems is at the elevation bearing regions. At node ⑤ (as at node ⑥) bar ⑤ – ⑦, bar ⑤ – ③ and bar ⑤ – ⑧ of the elevation wheel (Fig. 4) interferes with bar ⑤ – (51) in close proximity to the node. The Bonn engineer's solution was to offset bar ⑤ – (51) at the elevation bearing and modify the bar ⑤ – (51) into a shallow truss to account for the resulting end moment from the offset. Since this end moment exists only for wind forces in the X direction and for vibration modes in the same direction, this design trade-off seems to be the correct solution.

The azimuth wheel assemblies must be off-center mounted at nodes (50), (52), (54), and (55) with respect to the forces developed at the wheel/rail contacts. These moments must be accounted for in the practical design.

The elevation gear box compliance was simulated by bar ③ – (53), and the azimuth gearboxes by bar (50) – (70) (typical).

The side clearance between the elevation bearing pillow blocks and the bottom support cone bars of the reflector will determine the azimuth bearing diameter. This clearance must be studied together with clearance for bar (93) and the same cone bars in a layout.

V. Reflector Analysis Description

The iterative design procedure for the reflector structure started first with the effort to minimize the wind distortion RMS as the overall structural weight was revised to a designated intermediate structural weight number through designing cycles in the IDEAS program. Then, with the program constrained not to reduce any cross-sectional areas, weight was added to the final desired weight figure to reduce the gravity distortion RMS. This procedure was described in more detail in Ref. 1 and the resulting 64-m design figures are delineated in Fig. 5.

The distortion RMS was computed within the IDEAS program by best fitting the deflections of the work points supporting the reflective surface panels with a paraboloid (Ref. 8). Each deflection number was weighted by a function of the surface panel area the node represented. This should represent the uniform amplitude objective of the shaped reflector surface.

The symmetry of the reflector's configuration was maintained by "grouping" the bars required to be of the same cross-sectional areas as those in the same "group" in the IDEAS program.

Throughout the designing cycles that minimized the RMS distortions, the IDEAS program was checking the structural quality of each bar as well as adjusting the cross-sectional area for minimizing RMS. Based on the axial loading, and the input stress limitations and design equations recommended in Ref. 5, the cross-sectional area of each group was revised, if necessary, through each cycle to comply with the requirements. The amount of the change was limited to the selected ten maximum percentage for each design cycle.

The end result of the IDEAS cycles was a structural design of a reflector assembly of the desired structural weight with minimum wind distortion RMS for the selected wind load, and minimum gravity loading RMS. The wind loading used was for the back wind direction at 60 deg elevation that produced the largest pitching moment and the maximum surface distortion also. If the objective design weight was large enough, then all of the bars would pass the structural quality tests without compromising the wind distortion RMS and gravity loading RMS.

The largest axial loadings of the bars normally results from the limit wind loadings. One limit loading occurs at stow configuration with the wind at maximum speed. The other occurs at horizontal look configuration with the wind directly into the back of the reflector, and with the wind at maximum speed allowable for this case.

The stow wind speed for design was determined to be 44.1 m/s (100 mph) (Ref. 6) for the Goldstone location. It was based on statistical analyses of wind data throughout the United States using the probability of occurrence of once in 100 years with gust factors added per Ref. 6.

With the reflector at operating altitudes other than the stow case, the hoops are compressively loaded to their maximum with the reflector at horizon look and with wind into the back side. This is the result of the erection procedure where the hoops are the last to be installed between the ribs. Hence, at the erection altitude of zenith look, the hoops are at zero load. Consequently, the rotation to horizon look applies a negative gravity load that loads the hoops compressively. This compression loading is then added to the compression loading resulting from the wind force into the back of the reflector.

The wind forces on work points of the reflector structure were computed by a 1108 program that generated the NASTRAN force card images. Pressure difference coefficients, derived using the method described in Ref. 7, were input to the program with geometry data. These coefficients were then multiplied by the surface panel areas applicable to each workpoint to create the force card data. A 1.15 factor was used in the force card to account for the wind drag of the reflector structure in the vicinity of the workpoint. The drag forces on other parts of the reflector's structures were not accounted for in the distortion calculations.

The structural quality checks were made for all loadings with no additional load or safety factors with exceptions as follows:

(1) The compressive yield stress was input at 2.48×10^5 kN/m^2 (36,000 psi) for use of the ASTM A36 structural steel. The tensile yield stress was input at 2.07×10^5 kN/m^2 (30,000 psi) for a 20% safety factor. Since compressive stability governs the design because of long members used in reflectors, the tensile input values appeared to have little effect on the design.

(2) The standard air density was used with no factor used for Goldstone's elevation.

(3) Load reversal was assumed. This meant that all tensile forces were checked as compressive forces.

For all wind loads other than the stow wind case, 31.3 m/s (70 mph) wind was used to develop the wind forces.

With the servo drives designed to move the antenna at any altitude in winds of 23 m/s (50 mph), the maximum loading condition at 23 m/s (50 mph) is possible. For this case, the factor of safety computes to two based on the differences of wind velocities.

The design equations recommended in Ref. 5 are incorporated in the IDEAS program, which computes the maximum permissible compressive stresses with no safety factor included. The equations and their applicable scopes are described in more detail in the appendix. A limit of the length to the radius of gyration (L/r) of 200 is made in the IDEAS program, which is equivalent to stating that all bars are considered to be pin ended. Recommendations in Ref. 5 allow partially restrained connections with multiple bolt connections for bracing members with L/r ratios to 250. With the projected use of welded square tube members, stress calculations should produce answers on the conservative side.

The main effort in the reflector design is focussed on attaining low wind distortion RMS; in other terms, it is a stiffness design. The stresses from just gravity loadings should be low. Also, if the final structural weight is large for minimizing wind distortion, the structural quality calculations will increase the allowable wind speeds from 44.7 m/s (100 mph) for the stow case as well as for other altitudes cases.

VI. RF Boresight Pointing Analysis

The environmental loads on the antenna structures normally produce changes of the RF boresight directions, which result in pointing gain losses aside from the gain losses due to distortions of the reflective surfaces. The pointing errors of the primary reflector's distortion may be calculated using the computed parameters of the best fit paraboloid (Ref. 8) to the distortion vectors, and the displacements of the phase centers of the RF feed. Ray tracing as shown in Fig. 7, defines the change in the RF boresight direction.

With the primary reflector supported on nodes (2) and (3) of the alidade (Figs. 4 and 6), additional pointing errors were calculated from computed displacements of these nodes in the alidade model by loadings of reaction forces from the reflector analysis.

With the elevation angle encoders mounted at nodes (5) and (6) measuring the differential rotations of the alidade and the elevation bearing shafts of the elevation wheel truss, two presently uncorrectable errors occur with respect to the elevation angle measurements to ground. The first error is the twist in the elevation wheel truss between the rotations of nodes (2) and (3) and the elevation bearing shafts. The second error occurs as the alidade joints or nodes (5) and (6) carrying the encoder's housing rotate slightly from displacements from the loading.

Using the 64-m computer model delineated in Table 2, the best fit paraboloid data to many wind load distortions are given in Table 3 to suit labels shown on Fig. 7. The largest distortion RMS and boresight error results from back wind to elevation 60 deg, which is the same for YAW 120 deg at elevation 0 deg. Table 4 lists the rotations of the alidade members previously described for four wind loads that determine the RF boresight error values.

In addition to the gain losses from pointing error, the gain loss from offset or separation of the RF feed's phase center and the focus of the best fit paraboloid must be added. This offset gain loss can be computed by use of the radiation program (Ref. 9) resulting in straight line functions between the offset and the equivalent gain losses in distortion RMS values. The functions shown on Fig. 8 are for the F/D value of 0.4235 used for our studies and the equivalent RMS loss values are converted to gain losses by the Ruze equation.

VII. Alidade Analysis Description

The elevation wheel/alidade model shown in Fig. 4 was laterally (X and Y) constrained at node (51), the azimuth radial bearing position; vertically (Z) constrained at the four corner nodes (50), (52), (54) and (55), the azimuth thrust bearing positions; and rotationally constrained about the Z axis by four azimuth gearbox links to ground nodes.

Nodes (2) and (3) were loaded with CONM2 weights of the reflector assembly for analyzing the alidade for the effect of gravity loadings. The counterweight at (3) was also modeled with a CONM2 weight card. Then, the reactions resulting from the wind loadings of the reflector were added as force cards at nodes (2) and (3). For the horizontal look configuration, the elevation wheel was rotated with node (8) above node (7). Two bars were added to the elevation wheel to connect nodes (3) and (7) to the horizontal elevation gearbox link as shown in Fig. 6.

The design cycle of the elevation wheel/alidade model will be illustrated with computed values from an earlier study with the same configuration as shown in Fig. 4. First, the model was analyzed using the stress designing mode of the IDEAS program, where each bar is reduced to the minimum area satisfying the stress constraints of the design equations previously discussed. With the elevation wheel at zenith look, the reaction forces from the reflector model for the stow wind loads in the X and Y directions (Fig. 4), and the reaction forces for the 60-deg elevation with wind from the back were used as loads on the model. The computed displacements of nodes (2) and (3) for the stow wind loads after the stress designing mode is shown by the left most values of Fig. 9 plotted against the structural weight.

Next, the model was analyzed using the point designing mode with moment-type dummy forces applied at nodes (2) and (3) and using, first, the stow wind reaction loads in the -Y direction as the real loads. The IDEAS program then minimized the combined displacements of nodes (2) and (3) resulting from the real loads by appropriate changes in the cross-sectional areas, with the total weight as a constraint. Thus, as the total weight increase for five design cycles, the displacement results are shown as solid lines in Fig. 9 to the right of the first values computed by the stress mode.

The combined displacements of nodes (2) and (3), or the rotation of the line connecting the two nodes, is shown to decrease in the plane of the real and dummy loadings. However, the rotation in the normal plane or XZ plane was also reduced with the increased areas, but to a lesser degree.

To decrease the rotation in the XZ plane, design cycles using the dummy and real loads in the -X direction, with the cross-sectional areas constrained from any reduction, produced the result shown by the dotted lines in Fig. 9 with a slight weight increase.

Figure 10 illustrates the individual bar area increases throughout the previously described design cycles.

VIII. Natural Frequency Analysis

Natural frequency analyses using the IDEAS program were made on an earlier computer model with the same configuration, but with slightly different dimensions to the model described in this article. The results shown in Table 5 should be well within 10% of the values for the described model.

IX. Conclusions

The basic design problem in the reflector structure is compressive failure of the bars in the truss. Nominally, the structure at stow is calculated to just fail on occurrence of a maximum wind velocity in a 100-year mean recurrence interval period. However, there are in-built safety factors on the plus side consisting of (1) limit of length to radius of gyration ratio of 200 for all bars, (2) pin ends on all bars, (3) load reversals assumed in the computations leading to tension loads calculated as compressive loads, (4) sea-level dynamic pressures assumed for wind loading calculations, (5) the 100-year mean recurrence interval period recommended in Ref. 10 for use with permanent structures (the 50-year period is used for transmission towers in Ref. 5), (6) the bars that reach failure mode first are inside the highly redundant truss where redistribution of forces can occur, (7) the designing process in the IDEAS program for minimizing the RMS wind distortion adds areas to the critical bars that are also critical at stow wind condition. This may result in added safety factors for the stow case. The addition is a function of the final structural weight of the reflector.

It turns out that if the reflector structure is loaded only by its own weight and if all cross-sectional areas are reduced by the identical ratio to the original areas, the gravity distortion figure and the longitudinal stresses remains the same as before. The wind loading stresses will increase inversely by the ratio and, hence, the distortion RMS figure.

If a lighter weight reflector is desired, with the increased wind distortion RMS of a finished design, the IDEAS program will proceed with the redesign reducing the cross-sectional areas while maintaining the stress constraints for all loads and the gravity distortion RMS figure, if there are excess areas for wind loads.

At this point in design, a "stick" quad was mounted with its height about equal to the focal length, and the deflection figures for the node representing the apex of the quad was used as the deflection of the hyperboloid's focus point. Further design effort is needed in this area to upgrade this displacement number of the RF feed system. With strong emphasis on quad legs, and with minimum shadowing of the reflector that results in low vibrational frequencies of the whole quad, stability problems in a wind gusting atmosphere may be introduced without careful study of this problem.

Appendix
Structural Design Equations

The self-supporting steel transmission tower is a truss assembly of steel angles using bolts for connection means. The critical loadings are compressive instabilities of the truss members. Since these characteristics can be applied similarly to reflector structures, the design guides for the transmission towers (Ref. 5) should provide a sound basis for the structural design of reflector trusses. The recommendations of Ref. 5 reflect the experience of good practice and actual full-scale destruction tests on towers.

The two basic strength formulas with no safety factors calculates the allowable unit stress on the cross section of axially-loaded compression members.

Short column when $KL/r \leqslant C_c$

$$F_a = \left[1 - \frac{\left(\frac{KL}{r}\right)^2}{2\,C_c^2}\right] F_y \qquad (1)$$

$$KL/r = 60 + \frac{0.50\,L}{r} \text{ for } \frac{L}{r} \text{ up to and including } 120 \qquad (2)$$

Long column when $KL/r \geqslant C_c$

$$F_a = \frac{*1.97 \times 10^9}{\left(\frac{KL}{r}\right)^2} \qquad (3)$$

$$KL/r = \frac{L}{r} \text{ for } \frac{L}{r} \text{ from } 120 \text{ to } 200 \qquad (4)$$

$$C_c = \pi\sqrt{\frac{2E}{F_y}} = 126.1 \text{ for steel (A36)} \qquad (5)$$

where

K = restraint factor
L = length of column, m
r = radius of gyration, m
F_a = unit compressive stress, kN/m^2
F_y = modulus of elasticity, kN/m^2
E = modulus of elasticity, kN/m^2

*1.97×10^7 (kN/m^2) = 2.80×10^8 (psi)

The use of Eq. (2) in Eq. (1) accounts for normal framing eccentricities at both ends of a "short" column. Equation (2) reflects significant reductions in strength of the compression member that occurs in the intermediate range of slenderness from eccentricities, crookedness, and residual stresses. However, this reduction diminishes for still longer columns, and becomes relatively insignificant for L/r in excess of C_c.

For members with L/r in excess of C_c, Eq. (4) used in Eq. (3) signifies that both ends are unrestrained against rotation. This results in more conservative results as compared to the guide (Ref. 5), which allows partial restraints against rotation for joints made by multiple-bolt connections to a member considered to have adequate flexural strength to resist rotation of the joint. However, the members are not analyzed for drag load from the stow wind that produces bending stresses, which should be added to the axial stresses. Since the summed stresses for the above loading in a typical member of the reflector structure does not exceed the yield stress, the use of Eq. (3) and (4) is considered to be logical.

References

1. Levy, R., "Conceptual Studies for New Low-Cost 64-M Antennas," in the *Deep Space Network Progress Report 42-33*, Jet Propulsion Laboratory, Pasadena, Calif., pp. 55–61, June 15, 1976.

2. Katow, M. S., "Radio-Frequency Boresight Analysis of the Low-Cost 64-Meter Antenna," in the *Deep Space Network Progress Report 42-35*, Jet Propulsion Laboratory, Pasadena, Calif., pp. 128, 130, August 15, 1976.

3. Levy, R., "Iterative Design of Antenna Structures," in the *Deep Space Network Progress Report*, Technical Report 32-1526, Vol. XII, Jet Propulsion Laboratory, Pasadena, Calif., pp. 100–111, December 15, 1972.

4. *The NASTRAN User's Manual* (level 16.0), NASA SP-222(03), March 1976.

5. "Guide for Design of Steel Transmission Towers," *ASCE*, 1971. Prepared by the Task Committee on Analysis and Design of Structures of the Structural Division of the American Society of Civil Engineers.

6. Katow, M. S., "Proposed Modifications to the Wind Load Specification Applied to Ground Antennas," in the *Deep Space Network Progress Report 42-32*, Jet Propulsion Laboratory, Pasadena, Calif., pp. 65–69, April 15, 1976.

7. Katow, M. S., "Aerodynamic Static Differential Pressure Values for the 50 Percent Porous Reflector Dish," in the *Deep Space Network Progress Report 42-29*, pp. 60–65, Jet Propulsion Laboratory, Pasadena, Calif.

8. Katow, M. S., and Schmele, L. W., "Antenna Structures: Evaluation Techniques of Reflector Distortions," in *Supporting Research and Advanced Development, Space Programs Summary 37-40*, Vol. IV, pp. 176–184, Jet Propulsion Laboratory, Pasadena, August 31, 1966.

9. Bathker, D., "Radiation Pattern Programs," in *Computer Programs for Antenna Feed System Design and Analysis*, Edited by Ludwig, A., TR 32-979, Jet Propulsion Laboratory, Pasadena, Calif., April 15, 1967.

10. Task Committee on Wind Forces, "Wind Forces on Structures," *Trans. ASCE*, Vol. 126, Part II, 1961, pp. 1124–1198.

Table 1. 64-m DSS 14 surface panel data

Panel No.	Dimensions			Area, m^2 $(ft)^2$	Surface Accuracy, mm (in.)
	A, m	B, m	C, m		
2	2.10	1.87	4.01	7.96 (85.7)	1.08 (0.043)
3	1.87	1.59	4.73	8.18 (88.1)	1.07 (0.042)
4	1.59	1.35	3.94	5.79 (62.3)	1.00 (0.039)
5	1.35	1.11	3.86	4.75 (51.1)	0.88 (0.035)
6	2.22	1.82	3.15	6.36 (68.5)	0.81 (0.031)
7	1.83	1.28	4.23	6.58 (70.8)	0.83 (0.033)
8	1.28	0.77	3.92	2.66 (28.6)	0.46 (0.018)
9	1.54	0.81	2.79	2.26 (24.3)	0.43 (0.017)

Table 2. 64-m computer model data

SEQ	Description	Weight	
		kg x 10^{-4}	(kips)
1	Reflector with back-up cone, with Cassegrain cone, and quad-structural weight	29.48	(650.0)
2	Additional Cassegrain weight	1.74	(38.0)
3	Additional quad weight	0.64	(14.0)
4	Surface panels weight	5.73	(126.4)
5	Alidade structural weight	68.21	(1503.7)
6	Counterweight	13.37	(295.0)

Major missing weights = elevation gear and its supports and base stiffeners for alidade

SEQ	Load/wind description	Wind velocity		Distortion RMS	
		m/s	(mph)	mm	(in.)
1	Zenith look gravity off/on	–	–	0.15	(0.0058)
2	Horizon look gravity	–	–	0.20	(0.0078)
3	Zenith look gravity – set 36 deg	–	–	0.17	(0.0067)
4	Horizon look gravity – set 36 deg	–	–	0.10	(0.0038)
5	60 deg elevation – back wind	13.4	30	0.31	(0.0123)
6	90 deg elevation – side wind	13.4	30	0.21	(0.0081)
7	0 deg elevation – back wind	13.4	30	0.05	(0.0019)
8	0 deg elevation – into face	13.4	30	0.06	(0.0022)

Table 3. 64-m best fit data

Best fit data	Wind velocity = 13.4 m/s (30 mph)			
	El 60 deg back wind or El 0 deg yaw 120 mm (in.)		El 90 deg – stow mm (in.)	
Distortion – RMS	0.31	(0.012)	0.21	(0.008)
A – Z offset	0.05	(0.002)	0.00	(0.000)
B – axis rotation	0.000269 – rad		0.000221 – rad	
C – focal length – best fit	27.0993	– m	27.0984	– m
D – Y offset	12.80	(0.504)	10.90	(0.429)
E –	7.29	(0.287)	5.99	(0.236)
F – feed deflection	0.43	(0.017)	0.28	(0.011)
G –	5.51	(0.217)	4.90	(0.193)
H –	5.94	(0.234)	5.18	(0.204)
I –	4.75	(0.187)	4.14	(0.163)
J –	2.54	(0.100)	1.85	(0.073)
K – boresight error	0.000094 – rad		0.000068 – rad	

Table 4. 64-m alidade boresight error data from wind loadings

SEQ	Wind direction	② − ③ rotation × 10^4 rad	Elevation shaft rotation ⑤ × 10^4 ⑥ rad		Encoder housing rotation ⑤ × 10^4 ⑥ rad		Uncorrected elevation error ⑤ × 10^4 ⑥ rad		Elevation boresight error ⑤ × 10^4 ⑥ rad		Azimuth boresight error × 10^4 ⑤1 rad
1	Yaw 0 deg Elevation 60 deg Back wind 31.3 m/s 13.4 m/s	9.06 1.66	8.65 1.59	8.65 1.59	3.06 0.56	3.06 0.56	0.41 0.08	0.41 0.08	3.47 0.64	3.47 0.64	0.0
2	Yaw 120 deg Elevation 0 deg 31.3 m/s 13.4 m/s	-4.03	2.33	2.58	0.76	2.10	1.70	0.36	1.70 0.31	0.36 0.07	-2.10 -0.39
3	Yaw 0 deg Elevation 90 deg 44.7 m/s 13.4 m/s	10.78 0.97	10.65 0.96	10.65 0.96	4.45 0.40	4.45 0.40	0.13 0.01	0.13 0.01	4.58 0.41	4.58 0.41	0.0
4	Yaw 90 deg Elevation 90 deg 44.7 m/s 13.4 m/s	-3.76	-0.08	-0.31	1.87	-2.28	-0.11	0.11	1.76 0.16	-2.17 -0.20	0.0
	44.7 m/s 13.4 m/s								-3.76[a] -0.34	-3.76[a] -0.34	

[a]Cross-elevation error.

Table 5. 64-m reflector plus alidade natural frequencies

SEQ	Elevation angle, deg	First mode rotation motion axis	Natural frequency, Hz
1	90	Azimuth axis	1.28
2	90	Elevation axis	1.18
3	0	Reflector symmetric axis	1.11
4	0	Azimuth	1.37

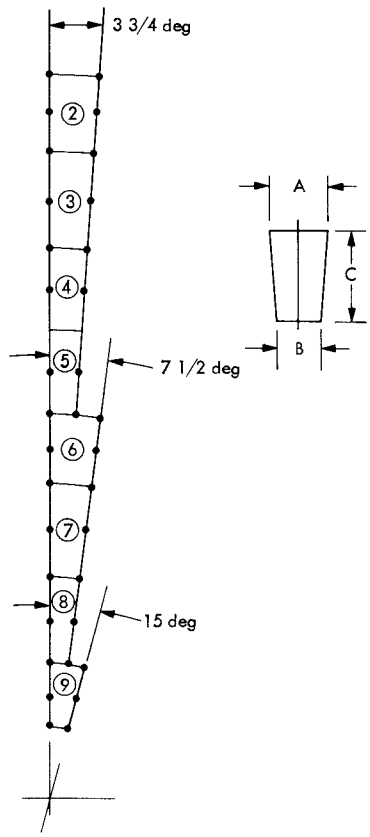

Fig. 1. 64-m antenna surface panels configuration, DSS 14

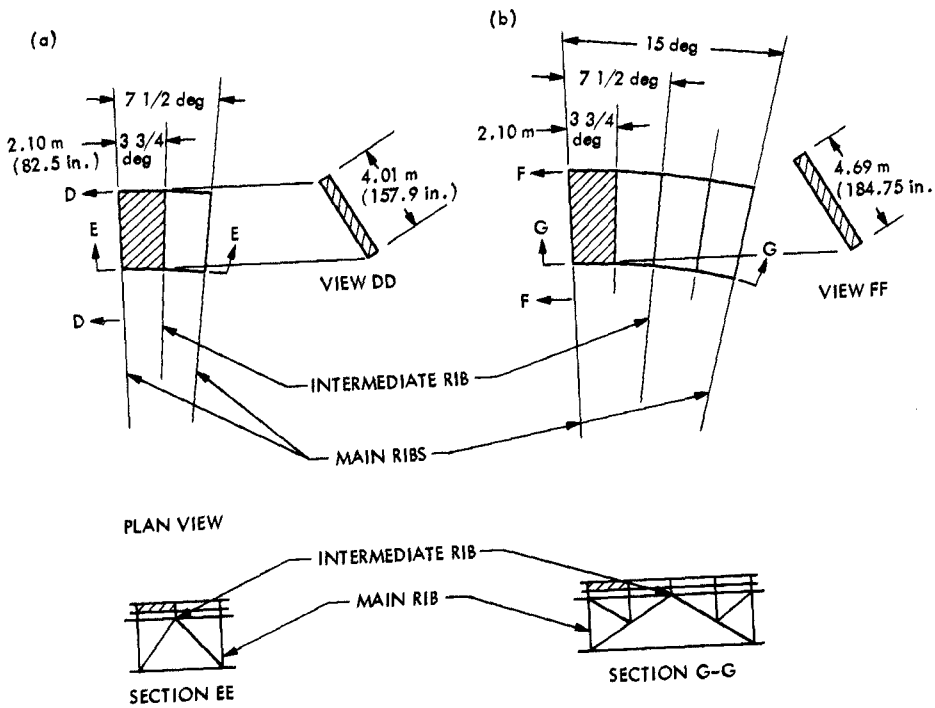

Fig. 2. Surface panel sizes: (a) 64-m, DSS 14; (b) 64-m, low cost

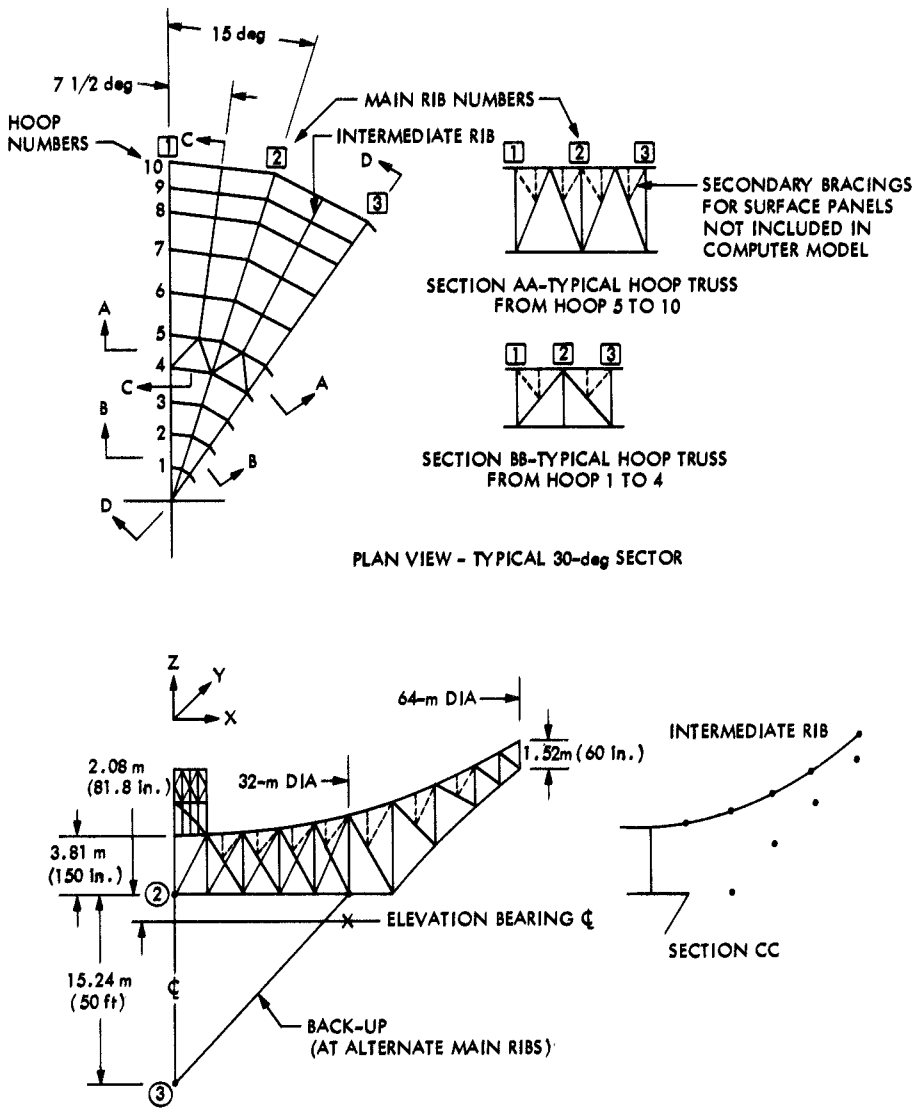

Fig. 3. 64-m low-cost reflector structural model

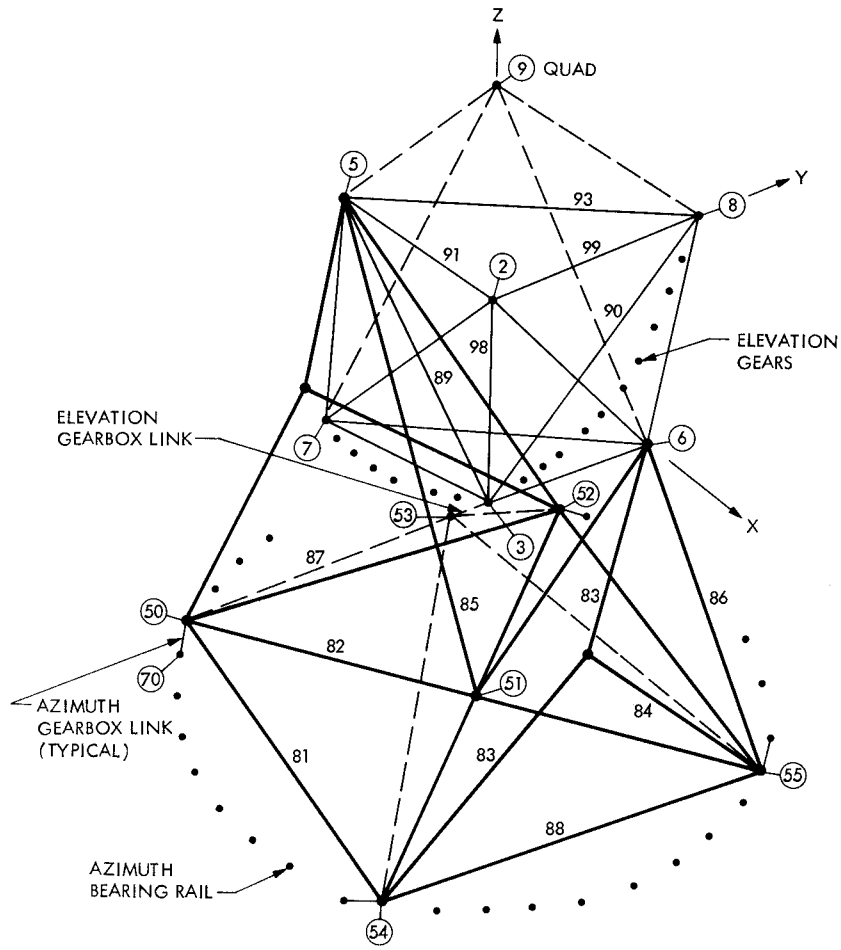

Fig. 4. Elevation wheel/alidade model

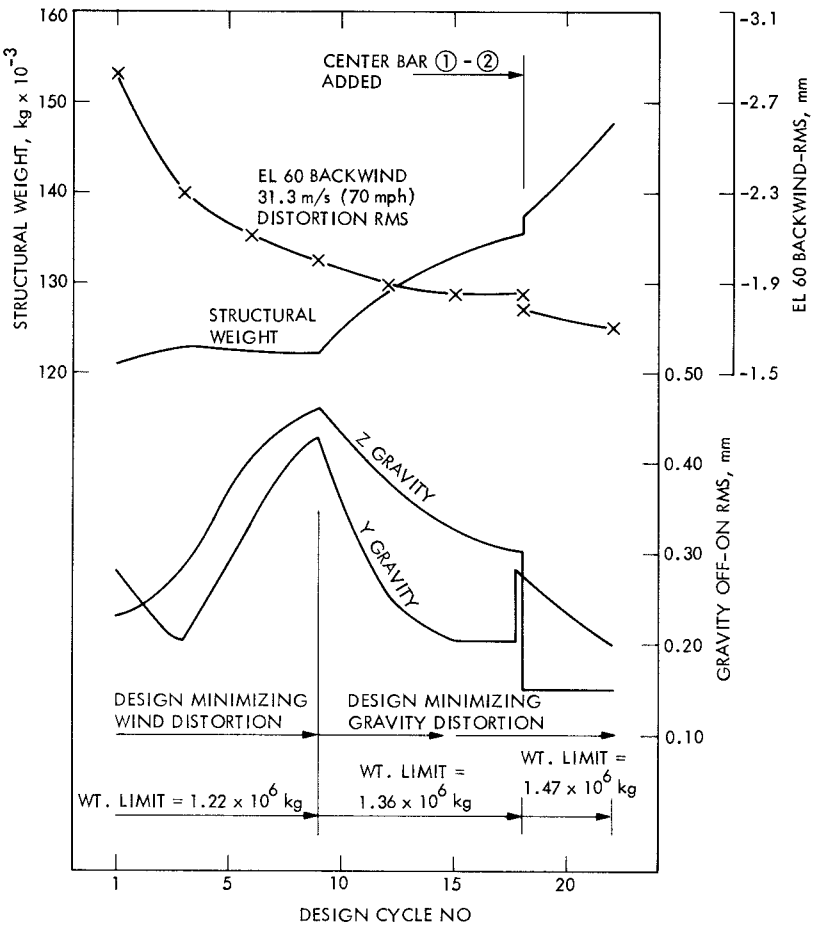

Fig. 5. 64-m IDEAS iterative design data

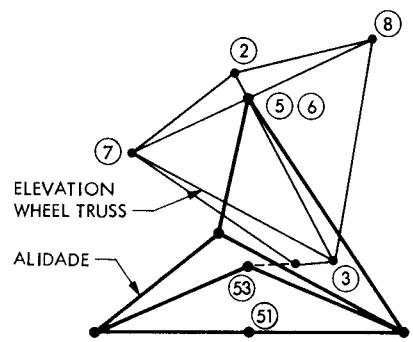

Fig. 6. Elevation wheel/alidade at 60-deg elevation

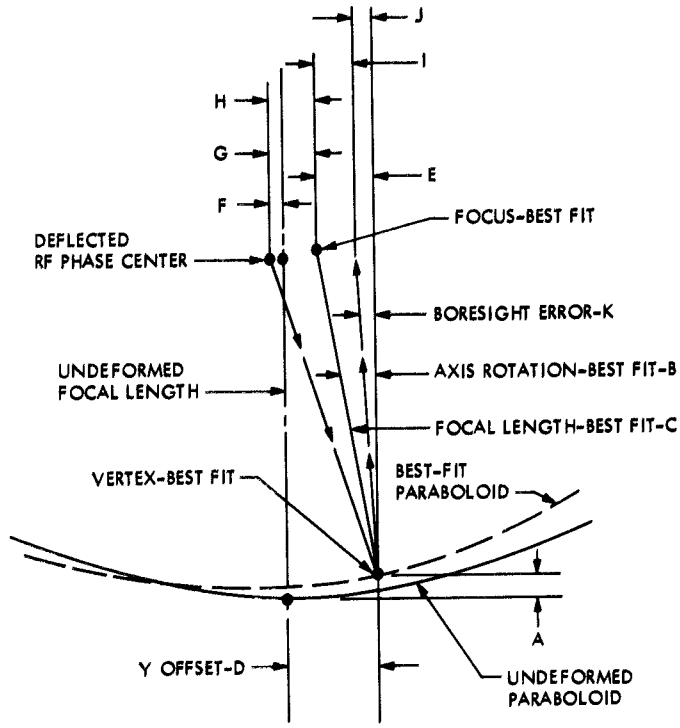

Fig. 7. 64-m reflector boresight error data

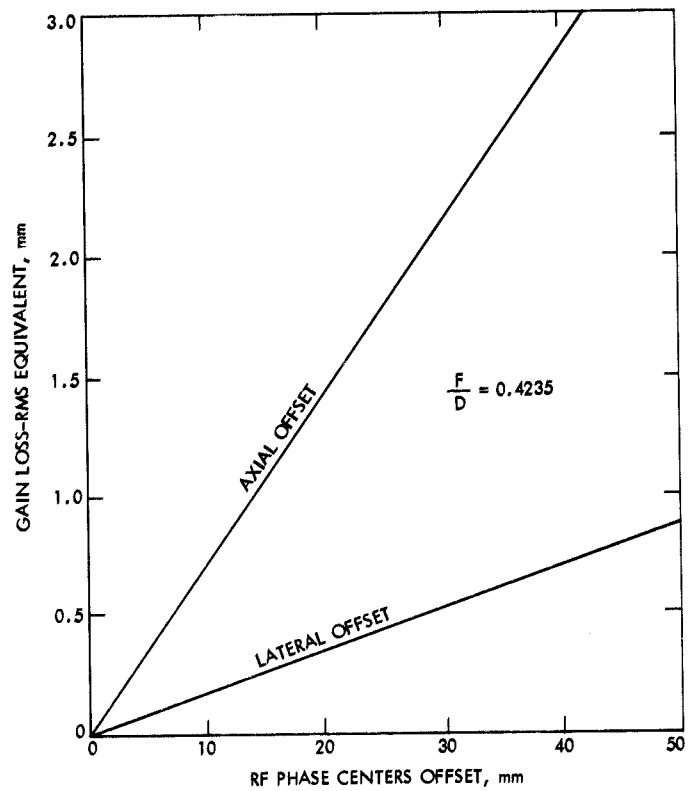

Fig. 8. Phase centers offset gain loss

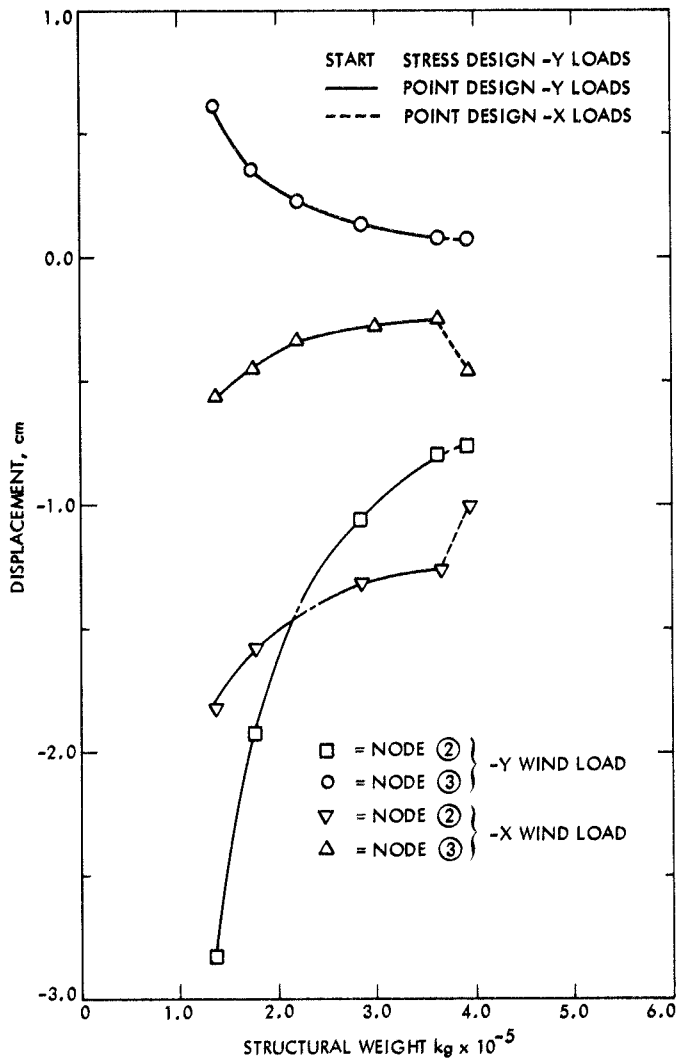

Fig. 9. 64-m alidade displacements vs design cycles

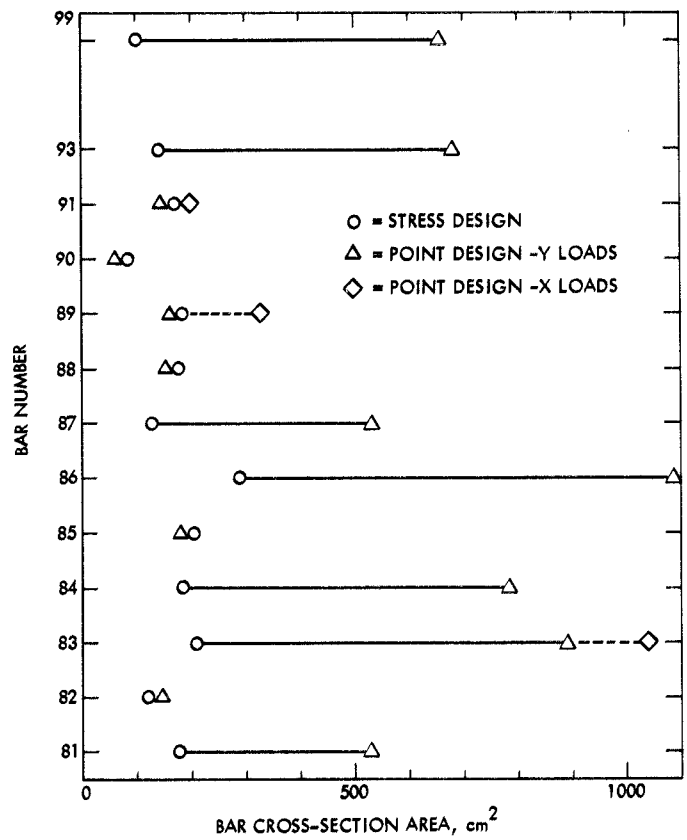

Fig. 10. Bar area changes - 64-m alidade design